

# Chiral surface twists and skyrmion stability in nanolayers of cubic helimagnets

A. O. Leonov,<sup>1,2,\*</sup> Y. Togawa,<sup>1,3</sup> T. L. Monchesky,<sup>4</sup> A. N. Bogdanov,<sup>1,2</sup> J. Kishine,<sup>1,5</sup>  
 Y. Kousaka,<sup>1</sup> M. Miyagawa,<sup>1</sup> T. Koyama,<sup>1</sup> J. Akimitsu,<sup>1</sup> Ts. Koyama,<sup>3</sup> K. Harada,<sup>3</sup> S.  
 Mori,<sup>3</sup> D. McGrouther,<sup>6</sup> R. Lamb,<sup>6</sup> M. Krajenak,<sup>6</sup> S. McVitie,<sup>6</sup> R. L. Stamps,<sup>6</sup> and K. Inoue<sup>1</sup>

<sup>1</sup>Center for Chiral Science, Hiroshima University, Higashi-Hiroshima, Hiroshima 739-8526, Japan

<sup>2</sup>IFW Dresden, Postfach 270016, D-01171 Dresden, Germany

<sup>3</sup>Osaka Prefecture University, 1-2 Gakuencho, Sakai, Osaka 599-8570, Japan

<sup>4</sup>Department of Physics and Atmospheric Science,

Dalhousie University, Halifax, Nova Scotia, Canada B3H 3J5

<sup>5</sup>The Open University of Japan, Chiba 261-8586, Japan

<sup>6</sup>School of Physics and Astronomy, University of Glasgow, Glasgow, UK, G12 8QQ

(Dated: October 8, 2018)

Lorentz transmission electron microscopy (LTEM) investigations of modulated states in a FeGe wedge and detailed calculations demonstrate that chiral twists arising near the surfaces of noncentrosymmetric ferromagnets (Meynell et al. Phys. Rev. B, **90**, 014406 (2014)) provide a stabilization mechanism for skyrmion lattices and helicoids in cubic helimagnet nanolayers. The calculated magnetic phase diagram for free standing cubic helimagnet nanolayers shows that magnetization processes in these compounds fundamentally differ from those in bulk cubic helimagnets and are characterized by the first-order transitions between modulated phases and the formation of specific multidomain states. The paper reports LTEM observations of multidomain patterns in FeGe free-standing nanolayers.

PACS numbers: 75.30.Kz, 12.39.Dc, 75.70.-i.

## I. INTRODUCTION

*Dzyaloshinskii-Moriya* (DM) interactions<sup>1</sup> stabilize two-dimensional axisymmetric solitonic states (*chiral skyrmions*) in saturated phases of magnetic materials with broken inversion symmetry<sup>2,3</sup>. In uniaxial noncentrosymmetric ferromagnets chiral skyrmions condense into hexagonal lattices below a certain critical field and remain thermodynamically stable (correspond to the global minimum of the magnetic energy functional) in a broad range of applied magnetic fields<sup>3</sup>. This does not occur in bulk cubic helimagnets where one-dimensional modulations along the applied field (the *cone* phase)<sup>4</sup> have the lowest energy practically in the whole area of the magnetic phase diagram, and skyrmion lattices can exist only as metastable states<sup>5,6</sup>.

During last years numerous observations of different types of skyrmion states have been reported in free-standing nanolayers and epilayers of cubic helimagnets (e.g.<sup>7-12</sup>). These findings have given rise to a puzzling question: why are skyrmion lattices totally suppressed in bulk cubic helimagnets but easily arise in nanolayers of the same compounds?

Two physical mechanisms have been proposed to date to explain the formation of skyrmion lattices in confined cubic helimagnets. One of them is based on effects imposed by induced uniaxial anisotropy<sup>5,6</sup>. In epilayers of cubic helimagnets on Si (111) substrates, a strong uniaxial anisotropy is induced by the lattice mismatch between the B20 crystal and the substrate<sup>6,13</sup>. This uniaxial anisotropy suppresses the cone phase and stabilizes a number of nontrivial chiral modulated states including out-of-plane and in-plane skyrmion lattices recently

observed in cubic helimagnet epilayers<sup>6,10,12</sup>.

The second stabilization mechanism is provided by specific modulations (*chiral twists*) arising near the surfaces of confined cubic helimagnets<sup>16-18</sup>. Chiral twists have been recently discovered in MnSi/Si(111) films<sup>16,18</sup>. However, their influence on the magnetic states arising in confined cubic helimagnets is still unclear. Also, physical mechanisms underlying the formation of skyrmionic states in free standing films of cubic helimagnets are unknown and a theoretical description of arising magnetic states in these systems is still an open question.

In this paper we report LTEM investigations of modulated states in a FeGe wedge and theoretical analysis of magnetic states in confined cubic helimagnets. Our findings show that surface twist instabilities play a decisive role in the stabilization of skyrmionic states in free standing layers of cubic helimagnets.

## II. PHENOMENOLOGICAL MODEL AND MAGNETIC PHASES

### A. Model

The standard model for magnetic states in cubic noncentrosymmetric ferromagnets is based on the energy density functional<sup>1,4</sup>

$$w = A (\mathbf{grad} \mathbf{m})^2 + D \mathbf{m} \cdot \mathbf{rot} \mathbf{m} - \mu_0 M \mathbf{m} \cdot \mathbf{H}, \quad (1)$$

including the principal interactions essential to stabilize modulated states: the exchange stiffness with constant  $A$ , Dzyaloshinskii-Moriya (DM) coupling energy with con-

stant  $D$ , and the Zeeman energy;

$$\mathbf{m} = (\sin \theta \cos \psi; \sin \theta \sin \psi; \cos \theta) \quad (2)$$

is the unity vector along the magnetization vector  $\mathbf{M} = \mathbf{m}M$ , and  $\mathbf{H}$  is the applied magnetic field.

We investigate the functional (1) in a film of thickness  $L$  infinite in  $x$ - and  $y$ - directions and confined by parallel planes at  $z = \pm L/2$  in magnetic field  $\mathbf{H}$  applied along  $z$ - axis (Fig. 1 a).

The equilibrium magnetic states in the film are derived by the Euler equations for energy functional (1) together with the Maxwell equations and with corresponding boundary conditions. The solutions depend on the two control parameters of the model (1), the *confinement ratio*,  $\nu$  and the reduced value of the applied magnetic field,  $h$

$$\nu = \frac{L}{L_D}, \quad h = \frac{H}{H_D}, \quad L_D = \frac{4\pi A}{|D|}, \quad \mu_0 H_D = \frac{D^2}{2AM} \quad (3)$$

where  $L_D$  is the *helix period* and  $H_D$  is the *saturation field*<sup>3,4</sup>.

### B. Modulated states in bulk cubic helimagnets

Magnetic states in bulk cubic helimagnets are commonly described by *unconfined* modulated states including the following three phases<sup>1,3,4</sup>:

(i) *Cones* are chiral single-harmonic modulations along the applied field. The solutions for the cone phase and the equilibrium energy density are derived in analytical form<sup>4</sup>

$$\cos \theta_c = h, \quad \psi_c = 2\pi z/L_D, \quad w_c(h) = -K_0 (1 + h^2) \quad (4)$$

where  $K_0 = D^2/(4A) = \mu_0 H_D M/2$  is the effective easy-plane anisotropy imposed by the cone modulations<sup>5,6</sup>.

(ii) *Helicoids* are one-dimensional chiral modulations with the propagation direction perpendicular to the applied field and homogeneous along the direction of the applied field<sup>1</sup>. Helicoids propagating along the  $x$ -axis are described by solutions  $(\theta(x), \psi = \pi/2)$ . The Euler equation for the helicoid energy density

$$w_h^0(\theta) = A \theta_x^2 - D \theta_x - \mu_0 M H \cos \theta \quad (5)$$

yields a set of parametrized periodic solutions  $\theta(x, l)$  where the parameter  $l$  designates the period of helicoids. The equilibrium period  $l_0$  and profile  $\theta(x, l_0)$  are derived by minimization of the helicoid energy density with respect to  $l$ <sup>1</sup>.

(iii) *Skyrmion lattices*. The axisymmetric cores of chiral skyrmion lattice cells are described by solutions<sup>3</sup>

$$\theta(\rho), \quad \psi = \pi/2 + \varphi \quad (6)$$

where  $\mathbf{r} = (\rho \cos \varphi, \rho \sin \varphi, z)$  are cylindrical coordinates of the spatial variable.

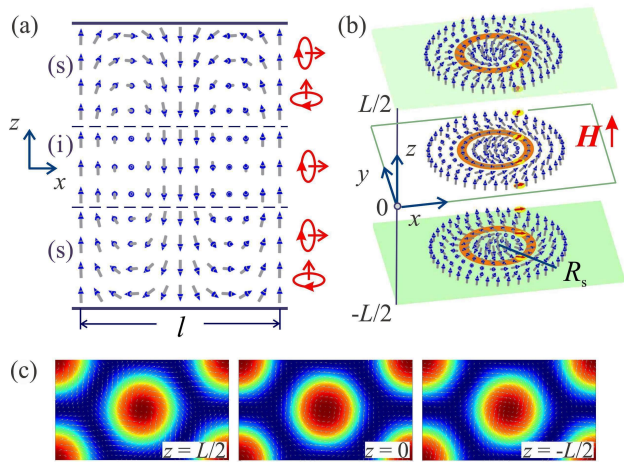


FIG. 1. (color online). Magnetic structure of a helicoid with period  $l$  (a) and a skyrmion lattice cell of radius  $R_s$  (b,c) in nanolayers of cubic helimagnets. In the internal area (i) the helicoid has in-plane modulations along the  $x$ -axis, the surface areas (s) are modulated along the  $x$  and  $z$  axes.

The equilibrium periods and magnetization profiles  $\theta(\rho)$  of the skyrmion lattice cells are derived by minimization of the energy density functional<sup>3</sup>

$$w_s^0(\theta) = A \mathcal{J}_s^0(\theta) + D \mathcal{I}_s^0(\theta) - \mu_0 M H \cos \theta, \quad (7)$$

$\mathcal{J}_s^0(\theta) = \theta_\rho^2 + \frac{1}{\rho^2} \sin^2 \theta$ ,  $\mathcal{I}_s^0(\theta) = \theta_\rho + \frac{1}{\rho} \sin \theta \cos \theta$  for different values of the core radii  $R$ , and optimization of the mean energy density of the skyrmion lattice with respect to  $R$ .

Among these solutions, the cone phase (4) corresponds to the global minimum of model (1) over the whole region where chiral modulations occur ( $H < H_D$ ). The helicoids and skyrmion lattices exist as metastable states below the critical fields  $H_h = 0.617H_D$  and  $H_s = 0.801H_D$  correspondingly<sup>1,3</sup>.

### C. Modulated states in confined cubic helimagnets

The solutions for unconfined helicoids (5) and skyrmion lattices (6) homogeneous along the film normal describe magnetic configurations in the depth of a bulk cubic helimagnet. However, the situation changes radically near the film surfaces. The gradient term,

$$m_x \partial m_y / \partial z - m_y \partial m_x / \partial z$$

in the DM energy functional (Eq. (1)) violates transversal homogeneity of helicoids and skyrmion states and imposes chiral modulations along the  $z$ - axis that decay into the depth of the sample (*surface twists*)<sup>6,16,17</sup>. The *penetration depth* of these surface modulations is comparable with the characteristic length  $L_D$ <sup>6</sup>.

Mathematically, axisymmetric skyrmion cells in thin films are described by solutions of type  $\theta = \theta(\rho, z), \psi =$

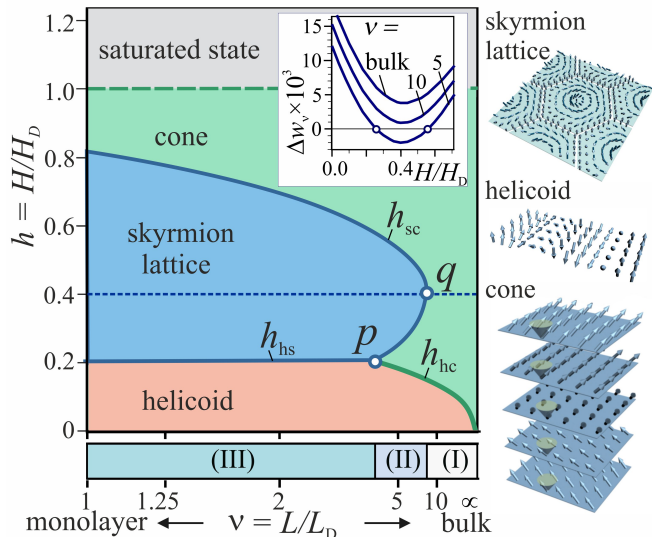


FIG. 2. (color online) The magnetic phase diagram of the magnetic states corresponding to the global minima for model (1) in reduced variables for the film thickness  $\nu = L/L_D$  and applied magnetic field  $h = H/H_D$ . The existence areas of the modulated phases (*cone*, *helicoids*, and *skyrmion lattice*) are separated by the first-order transition lines (solid).  $p$  (4.47, 0.232) is a triple point,  $q$  (7.56, 0.40) is a completion point. Dashed line indicates the second-order transition between the cone and saturated state. Along the dotted line  $H_a = 0.4H_D$ , the difference between the energy densities of the skyrmion lattice and the cone phase ( $\Delta w_\nu$ ) is minimal (Inset).

$\psi(\varphi, z)$ , and helicoids propagating in a film along the  $x$ -axis are described by solutions of type  $\theta(x, z), \psi(x, z)$ .

The energy density functional for confined helicoids ( $w_h(\theta, \psi)$ ) and skyrmion lattices ( $w_s(\theta, \psi)$ ) can be written in the following form

$$w_{h(s)} = A\mathcal{J}_{h(s)}(\theta, \psi) + D\mathcal{I}_{h(s)}(\theta, \psi) - \mu_0 MH \cos\theta, \quad (8)$$

where the exchange ( $\mathcal{J}_{h(s)}$ ) and Dzyaloshinskii-Moriya ( $\mathcal{I}_{h(s)}$ ) energy functionals read as

$$\mathcal{J}_h(\theta, \psi) = \theta_x^2 + \theta_z^2 + \sin^2\theta (\psi_x^2 + \psi_z^2),$$

$$\mathcal{I}_h(\theta, \psi) = \cos\psi\theta_x + \sin\theta\cos\theta\sin\psi\psi_x + \sin^2\theta\psi_z,$$

$$\mathcal{J}_s(\theta, \psi) = \theta_\rho^2 + \theta_z^2 + \sin^2\theta \left( \frac{1}{\rho^2}\psi_\varphi^2 + \psi_z^2 \right),$$

$$\mathcal{I}_s(\theta, \psi) = \sin(\psi - \varphi)(\theta_\rho + \frac{1}{\rho}\sin\theta\cos\theta\psi_\varphi) + \sin^2\theta\psi_z.$$

The equilibrium solutions for confined helicoids and skyrmion lattices are derived by solving the Euler equations for functional (8) with free boundary conditions at the film surfaces ( $z = \pm L/2$ ).

Most of the investigated free standing films and epilayers of cubic helimagnets have a thickness exceeding the period of the helix ( $L \geq L_D$ ). In this paper we carry out detailed analysis of the solutions for confined chiral modulations in cubic helimagnetic films with the thickness ranging from  $L = L_D$  to a bulk limit ( $L \gg L_D$ ).

### III. MAGNETIC PHASE DIAGRAM

#### A. Results of numerical simulations

The calculated  $\nu - h$  phase diagram in Fig. 2 indicates the areas with the chiral modulated states corresponding to the global minimum of the energy functional and separated by the first-order transition lines. For  $L \gg L_D$  the solutions for confined helicoids and skyrmion lattices approach the solutions for the magnetic states in the unconfined case(5), (6), which are homogeneous along the  $z$ -axis<sup>1,3</sup>. Surface twist instabilities arising in confined cubic helimagnets<sup>17,18</sup> provide a thermodynamical stability for helicoids and skyrmion lattices in a broad range of the applied fields (Fig. 2).

Another noticeable feature of the phase diagram is that the line  $h = 0.4$  is a symmetry axis for the skyrmion lattice stability area. This follows from the fact that in bulk helimagnets this field corresponds to the minimal value of the skyrmion lattice energy compared to that of the cone phase<sup>5,6</sup>. This effect plays a crucial role in the formation of the A-phase pocket near the ordering temperature of bulk cubic helimagnets (for details see the Ref.<sup>6</sup>). The differences between the equilibrium average energy densities of the skyrmion lattice ( $\bar{w}_s$ ) and the energy density of the cone phase ( $w_c$ )  $\Delta w_\nu(h) = \bar{w}_s(h, \nu) - w_c(h, \nu)$  plotted as functions of the applied field also reach the minimum in the fields close to  $h = 0.4$  (Inset of Fig. 2). As a result, below  $\nu_q = 7.56$ , the stability area of the skyrmion lattices extends around the line  $h = 0.4$ .

In the whole range of the film thickness, the helicoids with in-plane propagation directions correspond to the group state of the system. The triple point  $p$  (4.47, 0.232) and the completion point  $q$  (7.56, 0.40) split the phase diagram into three distinct areas with different types of the magnetization processes.

(I)  $\nu > \nu_q = 7.56$ . In these comparatively thick films, the helicoids remain thermodynamically stable at low fields and transform into the cone by a first-order process at the critical line  $h_{hc}(\nu)$ . The cone magnetization along the applied field increases linearly for increasing magnetic field up to the saturation at critical field  $H = H_D$ .

(II)  $4.47 = \nu_p < \nu < \nu_q = 7.56$ . In this case, the magnetic-field-driven evolution of the cone is interrupted by the first-order transition in the skyrmion lattice at  $h_{hc}(\nu) < h_q$  and the re-entrant transition at  $h_{hc}(\nu) > h_q$ .

(III)  $1 < \nu < \nu_p = 4.47$ . In this thickness range, the stability area of skyrmion lattices is separated from the low field helicoid and high field cone phases by the first order transition lines.

#### B. Analytical solutions for surface twists

In cubic helimagnet films with  $L \geq L_D$ , twisted modulations in helicoids and skyrmions ( $\xi(z)$ ) exist only in narrow regions near the film surfaces  $\delta \ll L$ . This allows us to write solutions for helicoids as  $\theta = \theta(x), \psi = \pi/2 + \xi(z)$

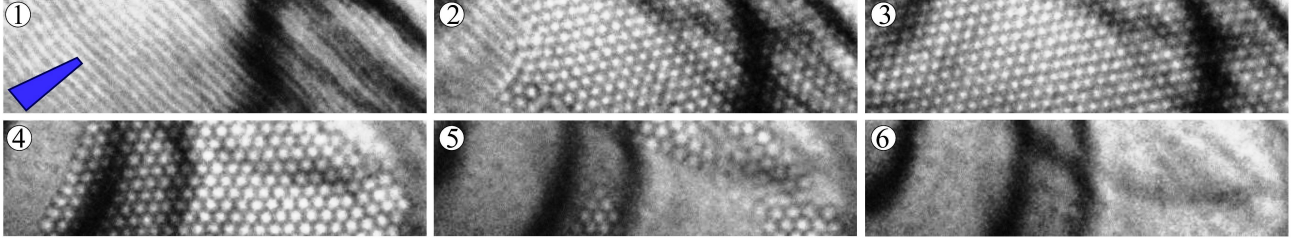


FIG. 3. LTEM images of modulated phases in a FeGe wedge at  $T = 250$  K and different values of the applied field  $H$  (Oe): 130 (1), 873 (2), 1073 (3), 2215 (4), 2355 (5), 3728 (6); fig. (3) indicates the coexisting helicoid and skyrmion lattice states and figs. (4), (5) the skyrmion lattice and cone domains during the first-order phase transitions. The image size is  $3000 \text{ nm} \times 800 \text{ nm}$ , the thickness varies from  $140 \text{ nm}$  (left) to  $60 \text{ nm}$  (right). Blue tetragons indicate the direction of the thickness gradients (in this and the next figures).

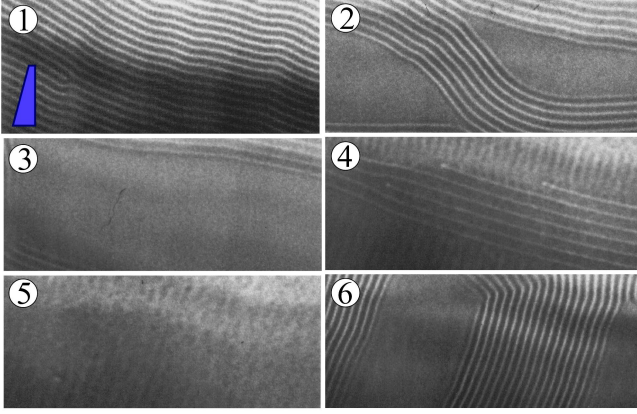


FIG. 4. (color online). LTEM images of a FeGe wedge at  $T = 110$  K for applied magnetic fields:  $H$  (Oe) = 200 (1), 1074 (2), 1460 (3), 3200 (4), 3670 (5), 200 (6) Figs. 2, 3 show the coexisting domains of the helicoid and cone state during the first-order transition between these phases. Multidomain states are restored after decreasing of the applied field (fig. (6)). The image size is  $3000 \text{ nm} \times 1250 \text{ nm}$ , the thickness varies from  $90 \text{ nm}$  (bottom) to  $60 \text{ nm}$  (top).

(the  $x$  axis is directed along the propagation direction), where  $\theta(x)$  is the solution homogeneous along the  $z$  axis investigated in<sup>1</sup>. We write the solutions for a skyrmion lattice core as  $\theta = \theta(\rho)$ ,  $\psi = \pi/2 + \varphi + \xi(z)$  where and  $\theta(\rho)$  is the solutions for skyrmions homogeneous along their axes<sup>3</sup>. The energy density of the surface twists in the helicoid (skyrmion lattice) can be reduced to the following form:  $e_{h(s)}(\xi) = \Delta \bar{w}_{h(s)}(\xi) = \langle m_x^2 \rangle_{h(s)} \mathcal{F}_{h(s)}(\xi)$  where

$$\mathcal{F}_{h(s)}(\xi) = \frac{2}{L} \int_0^\infty dz \left[ A \xi_z^2 - D \xi_z - K_0 v_{h(s)} \sin^2 \frac{\xi}{2} \right], \quad (9)$$

$K_0$  is the effective anisotropy (4), and

$$\langle m_x^2 \rangle_h = \frac{1}{l} \int_0^l \sin^2 \theta dx, \quad \langle m_x^2 \rangle_s = \frac{1}{\pi R_s^2} \int_0^{R_s} \sin^2 \theta \rho d\rho,$$

$$v_h = (4L_D/l) \langle m_x^2 \rangle_h^{-1}, \quad v_s = 2\eta_D (L_D/\pi) \langle m_x^2 \rangle_s^{-1},$$

$$\eta_D = \frac{1}{\pi R_s^2} \int_0^{R_s} \left( \theta_\rho + \frac{1}{\rho} \sin \theta \cos \theta \right) \rho d\rho.$$

The energy functional  $\mathcal{F}_{h(s)}(\xi)$  (9) describes surface twists  $\xi(z)$  in helicoids (skyrmion lattices) and has the same functional form as the energy functional for surface twists in a saturated helimagnet<sup>18</sup>. The Euler equation for (9) can be readily solved analytically. The equilibrium amplitude of twist modulations  $\xi(z)$  reaches the largest value on the film surface,

$$\xi_{h(s)}^{(0)} = 2 \arcsin \left( v_{h(s)}^{-1/2} \right) \quad (10)$$

and decays exponentially into the layer depth,

$$\tan(\xi_{h(s)}/4) = \tan(\xi_{h(s)}^{(0)}/4) e^{[-\pi \sqrt{v_{h(s)}}(z/L_D)]}. \quad (11)$$

Inserting (11) into the energy density (9) leads to the following expression for the *negative* energy density contribution imposed by surface twist modulations:

$$\bar{e}_{h(s)} = \underbrace{\langle m_x^2 \rangle_{h(s)} \left[ 2 \tan \left( \xi_{h(s)}^{(0)}/4 \right) - \xi_{h(s)}^{(0)} \right]}_{\sigma_{h(s)}} / L < 0. \quad (12)$$

The fractions of the *negative* surface contribution  $\bar{e}_{h(s)} \propto 1/L$  (12) in the total energy balance increase with decreasing film thickness, extending the stability areas of the helicoids and skyrmion lattices (2).

The magnetic phase diagram in Fig. 2 has been derived by minimization of the simplified (“isotropic”) energy functional (1) with *free* boundary conditions. This demonstrates how a *pure* geometrical factor (confinement) influences the energetics of cubic helimagnet nanolayers by imposing transverse chiral modulations (*twists*) in skyrmion lattices and helicoids. For the practically important thickness range  $L \geq L_D$ , the influence of chiral twists can be described by the surface energy term (12) in the cubic helimagnet energy.

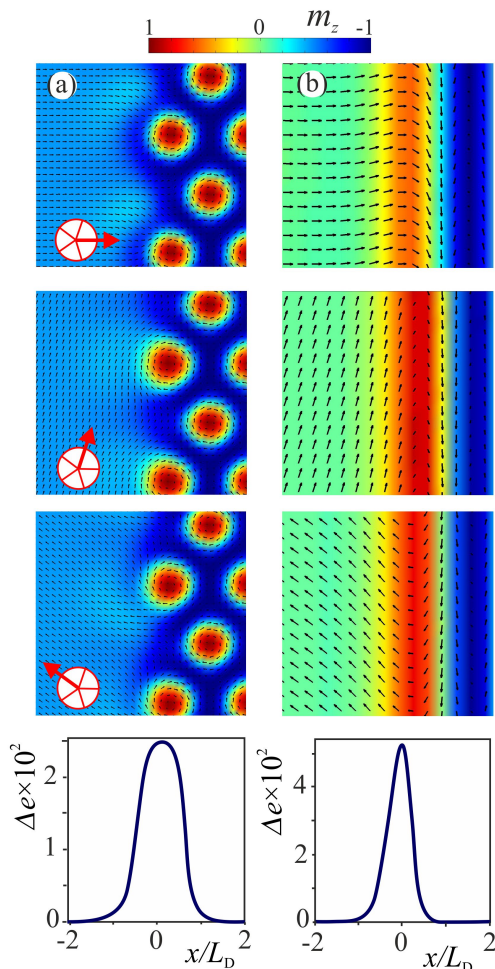


FIG. 5. (color online). Contour plots show the equilibrium structures of domain boundaries between the cone and the competing skyrmion lattice (a) and helicoid phases (b) during the first-order transition. The applied magnetic field is directed perpendicular to the figures planes. The domain wall between the cone and skyrmion lattice is calculated at the critical line  $h_{sc}(\nu)$  in the vicinity of the completion point  $q$  ( $h = 0.40$ ) (a), and the domain wall between the cone and helicoid at the transition line  $h_{hc}(\nu)$  for  $h = 0.01$  (b). The bottom panel shows the reduced energy density profiles through the domain wall thickness  $\Delta e(x) = |(w(x) - w_c(h))/w_c(h)|$  where  $w_c(h)$  is defined by Eq. (4).

#### IV. EVOLUTION OF SKYRMION AND HELICAL STATES IN A FE<sub>2</sub>GE WEDGE

Iron monogermanide FeGe belongs to a group of non-centrosymmetric cubic helimagnets with space group  $P2_13$  (B20-type structure)<sup>20,21</sup>. Below the Curie temperature  $T_C = 278.2$  K, FeGe is ordered into homochiral helices with period  $L_D = 70$  nm propagating along equivalent  $\langle 100 \rangle$  directions<sup>20</sup>. Below  $T_1 = 211$  K, helices propagate along  $\langle 111 \rangle$  directions. For increasing temperature, the propagation directions  $\langle 100 \rangle$  are restored at  $T_2 = 245$  K<sup>20</sup>.

In bulk cubic helimagnets, one-dimensional single-harmonic chiral modulations (helices and cones) are observed as stable states over practically the entire region below the saturation field<sup>20</sup>. Contrary to bulk specimens, in free standing nanolayers of cubic helimagnets with thickness  $L \leq 120$  nm investigated by LTEM methods, skyrmion lattices and helicoids are observed in broad ranges of applied magnetic fields and temperatures, while the cone phase is partially or completely suppressed<sup>7-9</sup>. Recent LTEM investigations represent an extensive study of the evolution of skyrmion states in confined cubic helimagnets (see e.g.<sup>7-9,25</sup> and bibliography in<sup>22</sup>).

In our paper we use LTEM to explore first-order phase transitions into the cone phase and other specific magnetization processes imposed by the *chiral surface twists* (Fig. 2). For our studies, we have prepared wedge-shaped single crystal FeGe(110) films. FeGe single crystals were grown by a chemical vapor transport method. A thin film specimen was made for TEM observations by using a focused ion beam technique. A series of Lorentz micrographs were taken by means of a Fresnel mode of Lorentz microscopy with a typical defocus value of 10 micrometer at  $T = 110$  K and 250 K in a broad range of magnetic fields applied perpendicular to the film surface (Figs. 3, 4). They clearly expose the magnetic-field-driven first-order transitions between the basic modulated states accompanied by the formation of the multidomain patterns composed of domains of the competing phases.

It should be noted that at LTEM images the domains of the cone phase appear as dark areas and cannot be distinguished from domains of the saturated state. However, in Figs. 3, 4, the dark domains arise at applied fields lower than the saturated fields (for FeGe, the saturation field  $\mu_0 H_D = 0.359$  T (3)<sup>20,21</sup>). Moreover, according to the theoretical results<sup>1,3</sup> and experimental observations<sup>7,14</sup>, the magnetic-field-driven transitions of the helicoid and skyrmion lattice into the saturated state advance gradually by the extension of the modulation period and formation of isolated helicoidal kinks and skyrmions. These processes exclude the formation of multidomain patterns of the competing phases characteristic of the first-order transitions<sup>15</sup>.

In Fig. 3, the layer thickness varies from  $L = 140$  nm ( $\nu = 2$ ) at the left edge to  $L = 60$  nm ( $\nu = 0.86$ ) at the right edge. In the calculated phase diagram, this thickness interval ( $0.86 < \nu < 2$ ) belongs to *area III* characterized by the first-order transitions between the helicoid and skyrmion lattice at the lower field,  $h_{hs}(\nu)$ , and between the skyrmion lattice and cone at higher field,  $h_{sc}(\nu)$  (Fig. 2). Both these phase transitions are clearly observed in Fig. 3. Because the transition field  $h_{sc}(\nu)$  has lower values for larger  $\nu$ , initially the cone phase nucleates at the thicker edge of the film (Figs. 3, (4)) and expands to the thinner part with an increasing applied field (Figs. 3, (5)).

The LTEM images derived at  $T = 110$  K (Fig. 4) have been done for a wedge area belonging to the same thickness interval as that in Fig. 3 with the thickness variation

from  $L = 90$  nm ( $\nu = 1.29$ ) at the bottom edge to  $L = 60$  nm ( $\nu = 0.86$ ) at the top edge. However, the magnetization evolution differs drastically from that observed at higher temperature. In this case, a skyrmion lattice does not arise, instead the helicoid directly transforms into the cone phase at a considerably lower field by a first-order process (Fig. 4 (2), (3)). In the  $(\nu, h)$  phase diagram (Fig. 2) such a magnetization evolution occurs in the *area I* for  $\nu > \nu_q = 7.56$ . The suppression of skyrmion lattices and helicoids at lower temperatures is characteristic for free-standing cubic helimagnet nanolayers<sup>8,9</sup>. Particularly, at  $T = 110$  K, the skyrmion lattices arise in FeGe free-standing layers only when their thickness is smaller than 35 nm<sup>8</sup>. This effect can be understood if we assume that the surface energy imposed by chiral twists  $\sigma_{h(s)}$  (12) decreases with decreasing temperatures. As a result, at lower temperatures the existence area of skyrmion lattices in the  $(\nu, h)$  phase diagram (2) would be shifted into the region of lower  $\nu$ .

Finally we consider specific domain wall separating domains of the competing modulated phases during the first-order transition. The transition between the helicoid and skyrmion lattice occurs in bulk and confined chiral helimagnets<sup>3,17</sup>. Domain walls between the coexisting helicoids and skyrmion lattices<sup>3</sup> have been observed in confined cubic helimagnets<sup>7,23,24</sup> and FePd/Ir bilayers<sup>26</sup>.

In the multidomain patterns in Figs. 3, 4 the domain boundaries between the cone phase and the helicoids and skyrmion lattices represent specific transitional areas providing the compatibility of the chiral modulations along the applied field (the cone) with the in-plane modulated phases. The contour plots in Fig. 5 describe the equilibrium structure of isolated domain walls between the cone and skyrmion lattice calculated for  $h = 0.4$  and between the cone and helicoid at  $h = 0$ . These calculations have been carried out for homogeneous along the film thickness domains of the helicoid and skyrmion lat-

tice phases. The energy density profiles of the domain walls in Fig. 5 show that the potential barriers separated the equilibrium modulated phases in domain are estimated as  $\Delta w_{max}(h) = \Delta e(0)|w_c(h)| \approx 10^{-2} K_0$ .

## V. CONCLUSIONS

The results of micromagnetic calculations for confined chiral modulations and LTEM investigations of magnetic states in a FeGe wedge demonstrate that chiral surface twists provide the stabilization mechanism for helicoids and skyrmion lattices in free standing cubic helimagnet films. For a practically important thickness range  $L \geq L_D$ , chiral twist modulations have sizable values only near the film surfaces and can be described analytically as localized surface states exponentially decaying into the film depth (Eqs. (10), (11)). The stabilization energy in this case is described by the surface energy contributions (12).

The solutions minimizing the energy functional (1) with free boundary conditions describe chiral modulations imposed solely by the *geometrical confinement* and expose three basic types of the magnetization processes in cubic helimagnet nanolayers (Fig. 2). In real system, however, the confined chiral modulations arise as a result of the interplay between the stabilization mechanism imposed by the geometrical confinement and other physical factors, such as intrinsic cubic anisotropy and induced volume and surface uniaxial anisotropy, internal and surface demagnetization effects. Our findings provide a conceptual basis for detailed experimental and theoretical investigations of the complex physical processes underlying the formation of skyrmion lattices and helicoids in confined noncentrosymmetric magnets.

\* A.Leonov@ifw-dresden.de

<sup>1</sup> I. E. Dzyaloshinskii, Sov. Phys. JETP **19**, 960 (1964), **20**, 665 (1964).

<sup>2</sup> A. N. Bogdanov and D. A. Yablonskii, Sov. Phys. JETP **68**, 101 (1989), <http://www.jetp.ac.ru/cgi-bin/e/index/r/95/1/p178?a=list>.

<sup>3</sup> A. Bogdanov and A. Hubert, J. Magn. Magn. Mater. **138**, 255 (1994), **195**, 182 (1999).

<sup>4</sup> P. Bak and M. H. Jensen, J.Phys. C **13**, L881 (1980).

<sup>5</sup> A. B. Butenko, A. A. Leonov, U. K. Rößler, A. N. Bogdanov, Phys. Rev. B **82**, 052403 (2010).

<sup>6</sup> M. N. Wilson, A. B. Butenko, A. N. Bogdanov, and T. L. Monchesky Phys. Rev. B **89**, 094411 (2014).

<sup>7</sup> X. Z. Yu, Y. Onose, N. Kanazawa, J. H. Park, J. H. Han, Y. Matsui, N. Nagaosa, and Y. Tokura, Nature **465**, 901 (2010).

<sup>8</sup> X. Z. Yu, N. Kanazawa, Y. Onose, K. Kimoto, W. Z. Zhang, S. Ishiwata, Y. Matsui, and Y. Tokura, Nature Mat. **10**, 106 (2011).

<sup>9</sup> X. Z. Yu, A. Kikkawa, D. Morikawa, K. Shibata, Y. Tokunaga, Y. Taguchi, and Y. Tokura, Phys. Rev. B **91**, 054411 (2015).

<sup>10</sup> M. N. Wilson, E. A. Karhu, A. S. Quigley, U. K. Rößler, A. B. Butenko, A. N. Bogdanov, M. D. Robertson, and T. L. Monchesky, Phys. Rev. B **86**, 144420 (2012).

<sup>11</sup> T. Yokouchi, N. Kanazawa, A. Tsukazaki, Y. Kozuka, A. Kikkawa, Y. Taguchi, M. Kawasaki, M. Ichikawa, F. Kagawa, Y. Tokura, J. Phys. Soc. Jpn. **84**, 104708 (2015).

<sup>12</sup> S. X. Huang and C. L. Chien, Phys. Rev. Lett. **108**, 267201 (2012).

<sup>13</sup> E. Karhu, S. Kahwaji, T. L. Monchesky, C. Parsons, M. D. Robertson, and C. Maunders, **82**, 184417 (2010); E. A. Karhu, S. Kahwaji, M. D. Robertson, H. Fritzsche, B. J. Kirby, C. F. Majkrzak, and T. L. Monchesky, Phys. Rev. B **84**, 060404 (2011).

<sup>14</sup> Y. Togawa, T. Koyama, K. Takayanagi, S. Mori, Y. Kousaka, J. Akimitsu, S. Nishihara, K. Inoue, A. S. Ovchinnikov, and J. I. Kishine, Phys. Rev. Lett. **108**, 107202

- (2012).
- <sup>15</sup> A. Hubert, R. Schäfer, *Magnetic Domains* (Springer, Berlin, 1998); V. G. Baryakhtar, A. N. Bogdanov, D. A. Yablonskii, *Sov. Phys. Usp.* **31**, 810 (1988).
- <sup>16</sup> M. N. Wilson, E. A. Karhu, D. P. Lake, A. S. Quigley, A. N. Bogdanov, U. K. Röbner, T. L. Monchesky, *Phys. Rev. B* **88**, 214420 (2013).
- <sup>17</sup> F. N. Rybakov, A. B. Borisov, A. N. Bogdanov, *Phys. Rev. B* **87**, 094424 (2013); F. N. Rybakov, A. B. Borisov, S. Blügel, N. S. Kiselev, *Phys. Rev. Lett.* **115**, 117201 (2015).
- <sup>18</sup> S. A. Meynell, M. N. Wilson, H. Fritzsche, A. N. Bogdanov, and T. L. Monchesky, *Phys. Rev. B* **90**, 014406 (2014).
- <sup>19</sup> L. Néel, *J. Phys. Rad.* **15**, 225 (1954).
- <sup>20</sup> B. Lebech, J. Bernhard, and T. Freltoft, *J. Phys.: Condens. Matter* **1**, 6105 (1989).
- <sup>21</sup> H. Wilhelm, M. Baenitz, M. Schmidt, C. Naylor, R. Lortz, U. K. Röbner, A. A. Leonov, and A. N. Bogdanov, *J. Phys.: Condens. Matter* **24**, 294204 (2012).
- <sup>22</sup> N. Nagaosa and Y. Tokura, *Nat. Nanotech.* **8**, 899 (2013).
- <sup>23</sup> J. Rajeswari, H. Ping, G. F. Mancini, Y. Murooka, T. Latychevskaia, D. McGrouther, M. Cantoni, E. Baldini, J. S. White, A. Magrez, T. Giamarchi, H. M. Roennow, F. Carbone, *PNAS* (2015).
- <sup>24</sup> M. Nagao, Y. So, H. Yoshida, K. Yamaura, T. Nagai, T. Hara, A. Yamazaki, and K. Kimoto, *Phys. Rev. B* **92**, 140415 (2015).
- <sup>25</sup> Y. Onose, Y. Okamura, S. Seki, S. Ishiwata, and Y. Tokura, *Phys. Rev. Lett.* **109**, 037603 (2012).
- <sup>26</sup> N. Romming, C. Hanneken, M. Menzel, J. E. Bickel, B. Wolter, K. von Bergmann, A. Kubetzka, and R. Wiesendanger, *Science* **341**, 636 (2013).